



Mechanistic aspects of the role of chelating agents in enhancing Fischer–Tropsch synthesis activity of Co/SiO₂ catalyst: Importance of specific interaction of Co with chelate complex during calcination

Naoto Koizumi^{a,*}, Yukiya Ibi^a, Daichi Hongo^a, Yusuke Hamabe^a, Shigenobu Suzuki^a, Yasuhiko Hayasaka^a, Takayoshi Shindo^b, Muneyoshi Yamada^c

^a Department of Applied Chemistry, Graduate School of Engineering, Tohoku University, Aoba 6-6-07, Aramaki, Aoba-ku, Sendai 980-8579, Japan

^b Department of Engineering in Applied Chemistry, Graduate School of Engineering and Resource Science, Akita University, 1-1 Tegatagakuen-machi, Akita 010-8502, Japan

^c Akita National College of Technology, 1-1, Iijima-Bunkyo-cho, Akita 011-8511, Japan

ARTICLE INFO

Article history:

Received 14 November 2011

Revised 9 February 2012

Accepted 10 February 2012

Available online 16 March 2012

Keywords:

Co/SiO₂ catalyst

Fischer–Tropsch synthesis

Chelating agent

CyDTA

Quick XAFS

ABSTRACT

Co/SiO₂ catalysts (20 mass%) with enhanced activities for Fischer–Tropsch synthesis (FTS) were prepared by a newly developed two-step impregnation method using several chelating agents, and the effects of the calcination temperature and chelating agent on their FTS activities were investigated to clarify the role of the chelating agent during preparation of the catalyst. Their effects upon coordination environments of Co species were also studied by in situ Co K-edge quick XAFS in conjunction with ex situ characterization techniques. The FTS activity of the catalysts increased with the calcination temperature, 473–543 K, when the chelating agents with strong affinity to Co²⁺ such as *trans*-1,2-diaminocyclohexane-*N,N,N',N'*-tetraacetic acid (CyDTA) were used for preparation. Such increase in the activity was accompanied with size reduction of Co species, while those in Co/SiO₂ prepared in the absence of the chelating agents were simply agglomerated during calcination. In situ quick XAFS suggested that size reduction of Co species was associated with specific interaction between small Co oxide clusters and chelate complexes during calcination. It was also speculated that these complexes were converted to surface silicate species after combustion of carbonaceous moieties which would work as anchoring sites of Co oxide clusters, preventing agglomeration of small Co₃O₄ species originated from the clusters during calcination at high temperatures.

© 2012 Elsevier Inc. All rights reserved.

1. Introduction

Co-based catalysts are well known as typical Fischer–Tropsch synthesis (FTS) catalysts, which synthesize mainly linear paraffins with a wide range of carbon numbers from CO and H₂. Nano-sized Co⁰ particles formed on catalyst surface under FTS conditions have been recognized to be the origin of their catalytic activity for hydrocarbon formations. Iglesia [1] reported that turnover frequencies (TOFs) of Co catalysts supported on SiO₂, Al₂O₃, and TiO₂ were similar and almost independent of size of the Co⁰ particles when they were larger than 10 nm. On the other hand, noticeable size effects of the Co⁰ particles were found in a small particle range (2–10 nm) for Co supported on carbon nanofiber [2,3] and ITQ-2 [4]. In these particle ranges, TOFs of these catalysts increased linearly with increasing Co⁰ particle size. These studies demonstrated that the Co-time yield (CTY; mole of CO converted per weight of Co

per second) increases with decreasing size of the Co⁰ particles at least up to 10 nm on conventional metal oxide support. Therefore, improvement of Co⁰ dispersion without loss of reducibility of Co is important strategy for enhancing their FTS activities.

Co-based FTS catalysts are usually prepared by impregnation of an aqueous solution containing Co(NO₃)₂·6H₂O on support materials followed by drying and calcination. During calcination, impregnated Co nitrate is decomposed to form Co₃O₄ species, and these precursor oxides are reduced by H₂ to the Co⁰ particles prior to FTS. Over the last two decades, many efforts have been devoted to develop an effective preparation method for improving dispersion of Co⁰ including, for example, adaptation of calcination procedures [5–9] and exploring new Co precursors instead of conventional Co nitrate [10–14]. Several researchers demonstrated that Co⁰ particles with smaller sizes were formed when the catalyst was prepared using Co oxalate [10] and a mixed salt of Co nitrate and Co acetate [11] as precursors. Unfortunately, however, use of these precursors produced significant amounts of Co silicate-like species simultaneously, which were hardly reduced to the metallic state under normal conditions. Therefore, reducibility of Co was suppressed greatly, resulting in only weak activity enhancements. In

* Corresponding author. Present address: Earth and Mineral Sciences Energy Institute, The Pennsylvania State University, C-211 Coal Utilization Laboratory, University Park, PA 16802, USA.

E-mail address: nxk20@psu.edu (N. Koizumi).

other words, trade-off relationships between dispersion of Co⁰ and reducibility of Co were reported in these previous works. It has been suggested that the formation of Co silicate-like species is associated with strong interaction between Co precursors and surface hydroxy groups during impregnation based on characterizations of the catalysts with low Co loadings [12–14].

On the other hand, some chelating agents are known to improve activities of Co- and Ni-based catalysts, which are typically used for hydrosulfurization of oil fractions in their sulfided forms [15–25]. In our previous works, these chelating agents were applied to preparation of Co/SiO₂ catalysts with enhanced FTS activities, in which the catalyst was prepared by impregnation of the aqueous Co nitrate solution containing one chelating agent (L; L-Co²⁺ = 1 mol mol⁻¹) selected from those with different complex formation constants (K_{Co}) followed by drying and calcination [26–29]. The FTS activity of these chelate-assisted catalysts showed a volcano-type dependency upon the $\log(K_{Co})$ of the chelating agents, and the maximum activity was attained by the catalyst prepared using the chelating agent with medium affinity to Co²⁺, namely nitrilotriacetic acid (NTA). The rate of CO conversion over the NTA-modified catalyst was three times as high as that over the catalyst prepared without using the chelating agents. Furthermore, use of NTA improved dispersion of Co⁰ by a factor of 3, whereas it hardly affected high reducibility of Co [27,29].

In spite of unique advantages of the co-impregnation method using the chelating agents, however, Co loading of the catalyst was limited to maximum of 5 mass% due to low solubility of the chelating agent in the presence of Co nitrate. To increase Co loading, a two-step impregnation method was newly developed in which the catalyst was prepared by consecutive impregnation-drying steps using two kinds of impregnation solutions by turns; one was an aqueous solution containing a chelating agent and the other was an aqueous solution of Co nitrate, followed by calcination of the dried catalyst. By this two-step impregnation method, Co loading of the catalyst was increased successfully up to 20 mass%, and their FTS activity was enhanced by 2- to 3-folds compared with that of the catalyst prepared in the absence of the chelating agent [30–33]. Interestingly, *trans*-1,2-diaminocyclohexane-*N,N,N',N'*-tetraacetic acid (CyDTA) with much higher affinity to Co²⁺ than NTA was more effective for enhancing the FTS activity in the two-step impregnation method. Besides, under constant Co loading of 20 mass%, the FTS activity of the catalysts prepared using CyDTA increased sharply with increasing CyDTA-Co²⁺ molar ratio from 0.06 to 0.25 and leveled off above these ratios [30,32]. Therefore, it was suggested that only a part of Co²⁺ in the catalysts participated in the complex formation with CyDTA, which was associated with such large activity enhancement caused by CyDTA. In other words, surplus Co would remain as Co nitrate, and Co nitrate and the complex would coexist in the dried catalyst, namely before calcination. These results imply importance of the chemistries involved in drying and calcination of the catalyst for activity enhancement caused by CyDTA [33]; however, details of the mechanism have not been figured out yet.

Co K-edge XAFS is a powerful tool for investigating the speciation and coordination environments of Co species in the Co-based FTS catalysts because they usually lack in long-range order. In previous works, Co K-edge XAFS was mainly applied to structural analysis of oxidized, reduced, and used catalysts regarding the precursor effects [34,35], support effects [36–38], promoter effects [35,37,39,40] and deactivation mechanism of the catalysts [41–43], while only a few papers have reported Co K-edge XAFS of the catalysts during each process of catalyst preparation [35,44]. In our recent work, in situ Co K-edge quick XAFS (QXAFS) coupled with temperature-programed oxidation (TPO) successfully disclosed the role of triethylene glycol (TEG) during preparation of TEG-modified Co/SiO₂ with enhanced FTS activities [44]. In spite

of its potential usefulness, however, in situ Co K-edge QXAFS of the chelate-assisted Co catalysts has never been reported yet.

In this work, therefore, 20 mass% Co/SiO₂ catalysts were prepared by the newly developed two-step impregnation method using several chelating agents, and the effects of the calcination temperature and chelating agent on their FTS activities were investigated under pressurized conditions to deepen our understanding of the role of the chelating agent. Their effects upon coordination environments of Co species were also studied by in situ QXAFS in conjunction with several ex situ characterization techniques including XRD, XPS, FT-IR, and conventional XAFS. Based on these results, mechanism for enhancing the FTS activity of Co/SiO₂ induced by the chelating agents is discussed.

2. Experimental

2.1. Preparation of catalysts

The catalysts studied in this work were prepared by the two-step impregnation technique. Details of the preparation procedures are reported elsewhere [30,32,33]. Briefly, SiO₂ powder (BET surface area: 224 m² g⁻¹, average pore diameter: 15 nm, pore volume: 1.24 mL g⁻¹, particle size: 150–250 × 10⁻⁶ m) was impregnated with an aqueous solution containing one chelating agent (L) selected from those listed in Table 1 followed by pre-drying at 333 K for 2 h under flowing dry air. This sample was then dried at 393 K and 3 h in an electric oven under static air. The dried sample was subsequently impregnated with an aqueous solution containing Co(NO₃)₂·6H₂O (Wako Pure Chemicals, purity > 99.5%) followed by the drying procedures under the same conditions. The sample was finally calcined in an electric furnace at 723 K for 4 h with a ramp rate of 1.0 K min⁻¹ under stagnant air conditions. Co loading of the catalysts was 20 mass% (SiO₂ weight basis), and the L-Co molar ratio was fixed at 0.25. The catalysts were also prepared by the co-impregnation method in accordance with the procedures reported previously (Co loading = 5 mass%, L-Co²⁺ molar ratio = 1) [26,27]. Hereafter, these catalysts are simply denoted as Co/L/SiO₂ (stepwise impregnation) and L-Co/SiO₂ (co-impregnation), respectively. Note that the “dried” and “calcined” catalysts in this work are defined as the catalysts that underwent the 1st and 2nd impregnation-drying cycles, and 1st and 2nd impregnation-drying cycles followed by calcination, respectively.

2.2. Activity test

The FTS activity and selectivity of the catalysts were studied under pressurized conditions using a high-pressure fixed-bed flow reactor system. The reactor consisted of a stainless steel tube with internal diameter of 7 mm and was placed in an electrically heated oven. The gases, H₂ (purity > 99.995%) and 33 vol.% CO/62 vol.% H₂/5 vol.% Ar (purity > 99.99995%), were used without further purification. The flow rate and pressure of these gases were regulated with mass flow controllers and a backpressure regulator. Typically, 0.1 g of the calcined catalyst mixed with glass beads was charged into the reactor and then reduced in a stream of H₂ under 773 K

Table 1

Chelating agents used for preparation of the catalyst and their logarithmic complex formation constants ($\log K_{Co}$).

Chelating agent	$\log K_{Co}$
Iminodiacetic acid (IDA)	6.95
Nitrilotriacetic acid (NTA)	10.38
Ethylenediamine- <i>N,N,N',N'</i> -tetraacetic acid (EDTA)	16.31
Triethylenetetramine- <i>N,N,N',N'',N''',N''''</i> -hexacetic acid (TTHA)	17.10
<i>Trans</i> -1,2-diaminocyclohexane- <i>N,N,N',N'</i> -tetraacetic acid (CyDTA)	18.92

for 6 h. After H₂ reduction, the catalyst was allowed to cool down to ambient temperature. The feed gas CO/H₂/Ar then flowed into the system at the pressure of 1.1 MPa, and the catalyst was heated to 503 K at ramp rates of 2.5 K min⁻¹ to 473 K followed by 1.0 K min⁻¹ to 503 K for the activity evaluation (*W/F* = 1.25 g-cat h mol⁻¹). Gaseous products were periodically sampled with computer-controlled gas samplers and analyzed by two on-line GCs after the reaction temperature reached 503 K. An on-line GC/TCD (Shimadzu, GC-8A) was used for analysis of CO, CO₂, and CH₄, while another on-line GC/FID (Shimadzu, GC-2014) was used for analysis of C₁–C₇ hydrocarbons. Ar was used as an internal standard for GC/TCD analysis. Liquid products were collected with an ice trap and analyzed by an off-line GC/FID (Agilent Technologies, Agilent 6850A) after synthesis. In this work, the FTS activity of the catalysts was expressed as the Co-time yield (CTY; mole of CO converted per g-Co per second). Since the catalysts studied in this work showed practically constant CO conversions above 7 h on stream, the CTYs were calculated using the conversions obtained at 7 h on stream. The product selectivity was calculated based on molar amounts of the products accumulated during 20 h on stream. The selectivity for hydrocarbon with carbon number *n* (C_{*n*} selectivity) was defined on a carbon molar basis as indicated below (*Y_n* = molar yield of hydrocarbon).

$$C_n \text{ selectivity} = \left(nY_n / \sum_n nY_n \right) \times 100 \quad (1)$$

2.3. H₂ chemisorption and TPR measurements

Effects of the calcination temperature and chelating agent on size of the Co⁰ particles formed in the reduced catalyst were studied by H₂ chemisorption and TPR. Diameter of Co⁰ particles was calculated assuming a hemispherical morphology of metallic particles and 1:1 hydrogen chemisorption on surface metallic Co atom. Details of the procedures and the measurement conditions were reported elsewhere [27,29].

2.4. XRD

XRD measurements were carried out using a MiniFlex powder X-ray diffractometer (Rigaku). CuKα radiation was used as the X-ray source with the X-ray tube operating at 30 kV and 15 mA. The observed diffraction peaks were assigned by referring to Joint Committee on Powder Diffraction Standards (JCPDS) data. The crystallite size of Co₃O₄ species was calculated by Debye–Scherrer Eq. (2) using (311) diffraction peak of Co₃O₄.

$$D_{hkl} = k_{hkl} \lambda / \beta_{hkl} \cos \theta \quad (2)$$

In this equation, λ is the wavelength of the X-rays ($\lambda = 0.15405$ nm), and β_{hkl} is the full width at half maximum (FWHM) of the diffraction peak. The shape factor (k_{hkl}) was equal to 0.9 in this work.

2.5. XPS

XPS was used to study the effect of the chelating agent on size (dispersion) of Co species formed in the dried and calcined samples. The sample was mixed with boron nitride powder (Wako Pure Chemicals purity > 99.5%) and pressed into self-supporting wafer. XPS measurements were carried out on a Scienta ESCA200 spectrometer with monochromatic AlKα line as an excited source. The pass energy and energy step were 150 eV and 0.05 eV, respectively, for all experiments. Charge shift was corrected using B1s binding energy (190.1 eV) of boron nitride. Background was subtracted from the spectrum using Shirley equation. The obtained spectrum was further deconvoluted using Gaussian functions to quantify chemical species present in subsurface region.

2.6. FT-IR

Interaction between Co and the chelating agent in dried and calcined catalysts was studied by FT-IR. The sample was diluted 100-folds with KBr powder and pressed into self-supporting wafer. FT-IR spectra were acquired using a Varian FTS-6000 FT-IR spectrometer in a transmission mode with spectral resolution and accumulation of 4 cm⁻¹ and 1024, respectively, under ambient conditions. The observed FT-IR spectrum was deconvoluted with Gauss functions using IGOR Pro software (Wave Metrics).

2.7. XAFS measurements

Co K-edge XAFS of the catalysts were measured at BL14B2 in SPring-8 synchrotron radiation facility (Harima, Japan) with ring energy of 8 GeV by quick XAFS mode in a transmission setup. The X-rays passed through a Si(111) double-crystal monochromator and focused onto the sample. The EXAFS data were collected in a transmission mode using *I*₀ and *I* ionization chambers filled with 100% N₂ and 15% Ar/N₂, respectively.

For ex situ measurements, the appropriate amount of the dried and calcined samples were diluted 10-folds with polyethylene glycol powder using a mortar and pestle and then pressed into self-supporting wafer (φ 10 mm) at 25 MPa for 3 min. The amount of the sample was adjusted so that Δvt of wafer fell within the range of 0.7–1.0. XAFS measurements were carried out under ambient temperature with 100 s dwell time unless otherwise stated. In some experiments, the spectra were acquired at 17–20 K using a He cryostat to improve the S–N ratio of EXAFS oscillation. Some reference Co compounds including polycrystalline Co(NO₃)₂·6H₂O, Co₃O₄, Co(C₂O₄)·2H₂O and α -Co₂SiO₄ prepared from stoichiometric mixture of Co₃O₄ and SiO₂ were also used for XAFS measurements under ambient conditions.

On the other hand, in situ QXAFS coupled with TPO was used to monitor change in coordination structures of Co during calcination. The dried sample was mixed with the equivalent amount of boron nitride powder and then pressed into self-supporting wafer (φ 10 mm) under medium pressure (12 MPa, 2 min). Thickness of this sample wafer was below 1 mm, which is indispensable for reducing diffusion resistance of gases into wafer. Sample wafer was placed in an in situ XAFS cell made of quartz, and then the cell was connected with a flow system equipped with mass flow controllers. The sample was heated from 373 to 623 K at a ramp rate of 1 K min⁻¹ followed by 10 K min⁻¹ in the range of 623–723 K under flowing 20% O₂/He (99.99995%, approximately 100 mL min⁻¹). XAFS spectra were acquired at every 180 s. Hereafter, the XAFS spectrum measured at *T* means that the spectrum was accumulated during $T \pm 1.5$ (15) K for $T \leq 623$ K ($623 \text{ K} < T \leq 723 \text{ K}$). Tail gas from the in situ cell was analyzed simultaneously with an on-line MS spectrometer during in situ QXAFS experiments.

2.8. XAFS analysis

The observed Co K-edge XAFS were analyzed in a conventional manner including background subtraction and normalization followed by Fourier filtering using a Rigaku XAFS data analysis system (REX2000). Contributions from coordination shells in the Fourier transformed $k^3\chi(k)$ were then inverse Fourier transformed with a Hanning-type window function into *k* space. Structural parameters of each coordination shell were determined by a non-linear least-squares fitting in *k* space. Backscattering amplitude and phase shift of a Co–O coordination shell were extracted from Fourier transformed $k^3\chi(k)$ of Co(NO₃)₂·6H₂O. Those of Co–O and Co–C coordination shells calculated by FEFF8.4 code [45] using the Co(C₂O₄)·2H₂O structure were also used in some fitting analysis. Details of curve fitting analysis were reported elsewhere [44].

Pattern-fitting analysis was also carried out for Co K-edge XANES of the catalysts to identify Co species in the catalysts. The R -factor defined by the following Eq. (3) was used to evaluate the quality of the fitting.

$$R_f (\%) = \left[\frac{\sum (I_{obs} - I_{cal})^2}{\sum (I_{obs})^2} \right] \times 100 \quad (3)$$

3. Results

3.1. Effect of calcination temperature on FTS activity

The effect of the calcination temperature on the FTS activity of the catalysts prepared using several chelating agents was investigated in order to deepen our understanding of the origin of the promoting effects induced by the chelating agents. In this experiment, dried Co/L/SiO₂ was calcined in an electric furnace at a ramp rate of 1 K min⁻¹. Once furnace temperature reached a desired calcination temperature, the calcined sample was allowed to cool down to ambient temperature. The FTS activity of the calcined sample was evaluated at 503 K and 1.1 MPa after H₂ reduction at 773 K.

Fig. 1 illustrates CTYs over the catalysts prepared using the chelating agents including IDA, NTA, EDTA, TTHA, and CyDTA as a function of the calcination temperature. The CTY decreased monotonically with an increase in the calcination temperature when the catalyst was prepared without using the chelating agent, namely Co/SiO₂. Such dependency upon the calcination temperature is similar to those reported previously [46–48], indicating that Co species are agglomerated to form large particles during calcination. On the other hand, the CTYs over Co/IDA/SiO₂ and Co/NTA/SiO₂ were fairly constant and independent of the calcination temperature in the range studied here. These catalysts showed higher activities than Co/SiO₂ when calcined at 723 K. Furthermore, the CTYs increased almost linearly with increasing the calcination temperature in the range of 473–543 K when EDTA, TTHA, and CyDTA were used for preparation of the catalyst. These results clearly show that high calcination temperatures (>473 K) are crucial for large activity enhancement induced by these chelating agents. Conversely, the FTS activities of uncalcined Co/L/SiO₂ were rather lower than that of Co/SiO₂. It is also stressed that the CTYs over Co/L/SiO₂ (L = EDTA, TTHA, and CyDTA) fall on the same line regardless of the structure of the chelating agents. Since these chelating agents have larger complex formation constants with Co²⁺ (log $K_{Co} \geq 16$) than others, strong affinity of the chelating agent with Co²⁺ is another important factor for large activity

enhancement caused by the chelating agents. The increase in the CTY implies that preparation of Co/SiO₂ using the chelating agents with the larger complex formation constants enhances dispersion of Co during calcination, leading to the higher FTS activities after H₂ reduction.

Fig. 2 compares CH₄ and C₅₊ selectivities over Co/SiO₂ and Co/CyDTA/SiO₂ calcined at different temperatures. The C₅₊ selectivity over Co/CyDTA/SiO₂ was lower than that over Co/SiO₂ when the catalysts were calcined at 523 K and lower temperatures. However, it increased with increasing the calcination temperature and reached 84 C-mol% at 723 K, which was comparable to that over the catalyst prepared in the absence of the chelating agent. Conversely, the CH₄ selectivity over Co/CyDTA/SiO₂ decreased slightly with the calcination temperature and finally was about 10 C-mol%.

3.2. Impact of the calcination temperature on size of Co species

The catalysts calcined at different temperatures were then analyzed by ex situ XRD and XPS to confirm the effect of the chelating agents on size (dispersion) of Co species formed in the calcined catalyst. Co/NTA/SiO₂ and Co/CyDTA/SiO₂ were chosen as the chelate-assisted catalysts for these experiments because of their typical dependencies of the FTS activities upon the calcination temperature.

3.2.1. Ex situ XRD

Fig. 3A–C shows the effect of the calcination temperature on XRD patterns of Co/SiO₂, Co/NTA/SiO₂, and Co/CyDTA/SiO₂. These figures also include the XRD pattern of polycrystalline Co₃O₄ as a reference. No diffraction peaks were observed in the XRD pattern of Co/SiO₂ without calcination, while several diffraction peaks originated from Co₃O₄ species emerged when it was calcined at the temperatures higher than 473 K. Crystallite size of Co₃O₄ species calculated by Debye–Scherrer equation increased from 29 nm to 39 nm with increasing the calcination temperature as tabulated in Table 2. Similarly, only the diffraction peaks of Co₃O₄ species were observed in the XRD patterns of calcined Co/NTA/SiO₂. However, crystallite size of Co₃O₄ species in this catalyst was smaller than those in Co/SiO₂ regardless of the calcination temperature and was fairly constant in the temperature range studied here (see Table 2). Furthermore, the diffraction peaks of Co₃O₄ were barely observed in the patterns of Co/CyDTA/SiO₂ only when it was calcined at 523 K and 723 K. Crystallite size of Co₃O₄ species in the catalyst calcined at 523 K was no more than 7 nm and increased by only 2 nm even after calcination at 723 K as summarized in Table 2. It is noted that the catalysts studied in this work were calcined under stagnant air conditions, which resulted in

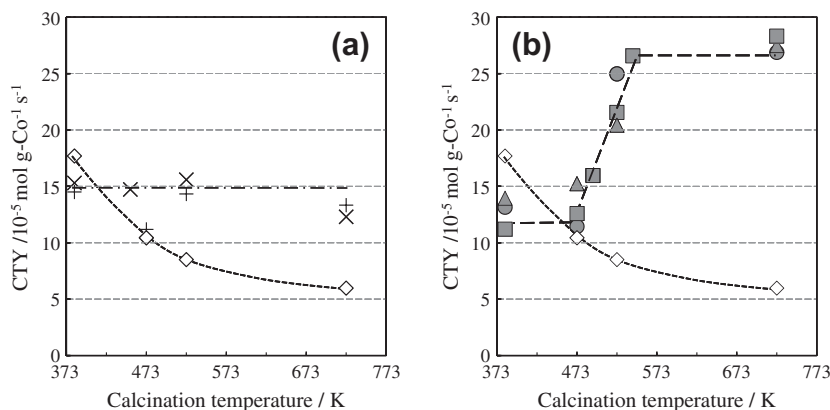


Fig. 1. Importance of the calcination temperature for enhancing the Co-time yield (CTY) over Co/SiO₂ prepared by a two-step impregnation method using chelating agents with various complex formation constants (see Table 1): Co/SiO₂ (open diamond), Co/IDA/SiO₂ (×), Co/NTA/SiO₂ (+), Co/EDTA/SiO₂ (closed circle), Co/TTHA/SiO₂ (closed triangle), Co/CyDTA/SiO₂ (closed square) FTS: 503 K, 1.1 MPa, W/F = 1.25 g-cat h mol⁻¹.

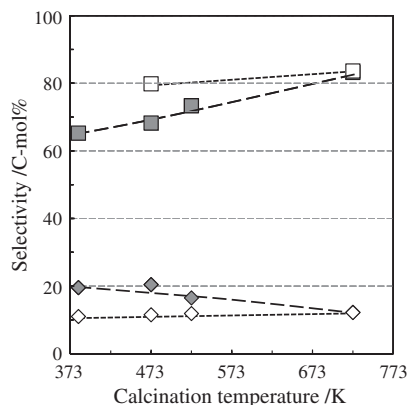


Fig. 2. CH₄ and C₅₊ selectivities over Co/SiO₂ and Co/CyDTA/SiO₂ calcined at different temperatures: CH₄ selectivity (diamond), C₅₊ selectivity (square), Co/SiO₂ (open symbols), Co/CyDTA/SiO₂ (closed symbols). Reaction conditions are the same as those indicated in Fig. 1.

the formation of Co₃O₄ species with large crystallite size in the absence of the chelating agents. On the other hand, those with much smaller size were observed in the catalyst calcined under N₂ flow (ca. 10 nm in 20 mass% Co/Al₂O₃) [6] or 1% NO/He flow (4–5 nm in 18 mass% Co/SiO₂) [7], respectively. In particular, size of Co₃O₄ species formed in the latter catalyst is even smaller than those formed in the calcined catalyst prepared in the presence of CyDTA. Therefore, optimization of the calcination conditions would be promising for improving dispersion of Co₃O₄ species in calcined Co/CyDTA/SiO₂ further, and the effect of the calcination conditions is now under investigation.

Hydrogen chemisorption capacity and TPR profiles were then measured on several catalysts, and diameter of the Co⁰ particles formed after H₂ reduction at 773 K was calculated (see parentheses in Table 2). Small Co⁰ particles with diameter of 5 nm were formed in Co/CyDTA/SiO₂ calcined at 523 K and grew slightly when calcined at the higher temperature. Among the catalysts calcined at 723 K, diameter of the Co⁰ particles decreased in following order, Co/CyDTA/SiO₂ (7 nm) > Co/NTA/SiO₂ (13 nm) > Co/SiO₂ (30 nm).

3.2.2. Ex situ XPS

Since small Co species would escape from XRD analysis, XPS was also used to evaluate size of Co species in the dried and calcined catalysts. After deconvolution of the ex situ XPS spectrum, the integrated intensity ratio of Co2p_{3/2} to Si2p, hereafter simply denoted as $I(\text{Co}2p_{3/2})/I(\text{Si}2p)$, was calculated and used for investigating change in size of Co species during calcination. In Fig. 4,

$I(\text{Co}2p_{3/2})/I(\text{Si}2p)$ for Co/SiO₂, Co/NTA/SiO₂, and Co/CyDTA/SiO₂ are plotted as a function of the calcination temperature. As expected from the XRD results, the $I(\text{Co}2p_{3/2})/I(\text{Si}2p)$ for calcined Co/SiO₂ decreased with increasing the calcination temperature from 473 K to 523 K which indicates that Co species are agglomerated to form large particles in this temperature range. On the other hand, the $I(\text{Co}2p_{3/2})/I(\text{Si}2p)$ for Co/L/SiO₂ (L = NTA, CyDTA) changed in different ways during calcination, that is, the $I(\text{Co}2p_{3/2})/I(\text{Si}2p)$ was almost constant and independent of the calcination temperature when NTA was used for preparation. More interestingly, the $I(\text{Co}2p_{3/2})/I(\text{Si}2p)$ for calcined Co/CyDTA/SiO₂ increased sharply with increasing the calcination temperature from 453 to 523 K and then turned to slight decrease by further increase of the calcination temperature. This sharp increase in the $I(\text{Co}2p_{3/2})/I(\text{Si}2p)$ suggests that relatively large Co species in dried Co/CyDTA/SiO₂ turn into smaller ones during calcination. It is also highlighted that the $I(\text{Co}2p_{3/2})/I(\text{Si}2p)$ for Co/CyDTA/SiO₂ decreases only slightly even after calcination at high temperatures, 523–723 K. This is consistent with the ex situ XRD results which showed that crystallite size of Co₃O₄ species in calcined Co/CyDTA/SiO₂ increased by only 2 nm after calcination at 723 K (see Table 2).

These changing behaviors of the $I(\text{Co}2p_{3/2})/I(\text{Si}2p)$ for Co/NTA/SiO₂ and Co/CyDTA/SiO₂ were mostly consistent with those observed in the FTS activity and crystallite size of Co₃O₄ species formed in the corresponding catalysts. In this connection, it is stressed that the $I(\text{Co}2p_{3/2})/I(\text{Si}2p)$ for dried Co/L/SiO₂ (L = NTA, CyDTA) were smaller than that for dried Co/SiO₂. This indicates that relatively larger Co species are formed in these chelate-assisted catalysts which would be related with the fact that uncalcined Co/L/SiO₂ showed the lower FTS activities than the catalyst prepared in the absence of the chelating agent. However, a discrepancy also arose between crystallite size of Co₃O₄ species and $I(\text{Co}2p_{3/2})/I(\text{Si}2p)$ for calcined Co/NTA/SiO₂; crystallite size of Co₃O₄ species in Co/NTA/SiO₂ calcined at 473 K was smaller than that in Co/SiO₂ calcined at the same temperature, while the $I(\text{Co}2p_{3/2})/I(\text{Si}2p)$ for the former sample was smaller than that for the later one. It is worth noting that Co/NTA/SiO₂ calcined at 473 K was a heterogeneous mixture of black and purple powder which indicated that crystalline Co₃O₄ species (black powder) coexisted with other non-crystalline Co species (purple powder) in this sample. Since only crystalline species are detected by XRD analysis, different sensitivities of XRD and XPS could cause such discrepancy mentioned above.

3.3. Interaction between Co and chelating agent during calcination

Mechanistic aspects of the roles of the chelating agents (NTA and CyDTA) during calcination were studied in view of interaction

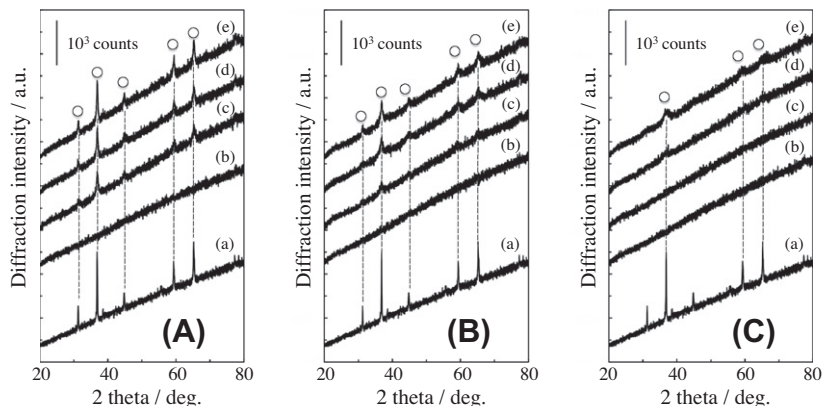


Fig. 3. Effect of the calcination temperature on ex situ XRD patterns of Co/SiO₂ (A), Co/NTA/SiO₂ (B) and Co/CyDTA/SiO₂ (C). Diffraction peaks of Co₃O₄ are indicated by open circle: Polycrystalline Co₃O₄ (a), after drying at 383 K (b), after calcination at 473 K (c), 523 K (d) and 723 K (e).

Table 2

Crystallite size of Co_3O_4 species formed in the calcined catalysts and diameter of Co^0 particles formed after H_2 reduction at 773 K.

Calcination temperature (K)	Crystallite size ^a (diameter ^b) (nm)		
	473	523	723
Co/SiO ₂	29	35	39 (30)
Co/NTA/SiO ₂	23	20	25 (13)
Co/CyDTA/SiO ₂	–	7 (5)	9 (7)

^a Crystallite size of Co_3O_4 species calculated by Eq. (2).

^b Diameter of Co^0 particles calculated by hydrogen chemisorption capacity and reduction degree of Co.

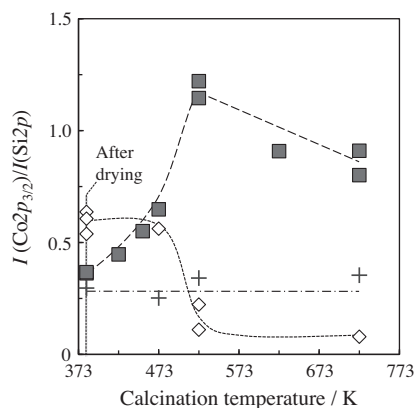


Fig. 4. Impact of the calcination temperature on the $I(\text{Co}2p_{3/2})/I(\text{Si}2p)$ ex situ XPS intensity ratio for Co/SiO₂ (open diamond), Co/NTA/SiO₂ (+), and Co/CyDTA/SiO₂ (closed square).

between Co and the chelating agents by means of ex situ FT-IR spectroscopy. FT-IR spectroscopy is a suitable technique for this purpose because it can easily distinguish chelate complexes from corresponding free chelating ligands.

3.3.1. Co/SiO₂

Fig. 5A illustrates FT-IR spectra of dried and calcined Co/SiO₂. In these spectra, only a broad band of $\delta\text{H}_2\text{O}$ was observed at 1631 cm^{-1} . The intensity of this band decreased with the calcination temperature, indicating that dehydration of the catalyst takes place during calcination.

3.3.2. Co/NTA/SiO₂

Fig. 5B demonstrates change in FT-IR spectra of Co/NTA/SiO₂ during calcination. In the FT-IR spectrum of the dried sample, a weak IR band was observed at 1590 cm^{-1} in addition to the band of $\delta\text{H}_2\text{O}$ at 1630 cm^{-1} . The band at 1590 cm^{-1} was also observed in the spectra of the catalysts calcined at 453–493 K, while it disappeared from the spectrum when the catalyst was calcined at 523 K. In this figure, the spectrum of dried NTA/SiO₂ is also included (Fig. 5B-f), which showed no clear bands at around 1590 cm^{-1} . In other words, the IR band at 1590 cm^{-1} was observed only when NTA coexisted with Co nitrate.

An aqueous solution containing NTA and Co nitrate with NTA- Co^{2+} molar ratio of unity was then prepared and characterized by FT-IR to study interaction between Co and NTA during calcination of the catalyst (Fig. 5B-g). It is known that a $[\text{CoL}]^-$ ($\text{L} = \text{NTA}$) complex is only stable Co species in the aqueous solution containing Co^{2+} and NTA in a wide pH range ($1 \leq \text{pH} \leq 14$) [49]. The spectrum of the reference solution adjusted to pH 10 showed a weak band at 1590 cm^{-1} that was assigned to $\nu_{\text{as}}\text{COO}^-$ of the $[\text{CoL}]^-$ complex [50]. Since the similar IR band was observed in the spectrum of the dried sample, it is suggested that interaction between NTA

and Co^{2+} in dried Co/NTA/SiO₂ is similar to that of the $[\text{CoL}]^-$ complex in the aqueous solution. This interaction was preserved during calcination up to 493 K. Above this calcination temperature, the band at 1590 cm^{-1} disappeared from the FT-IR spectrum, indicating decomposition of the complex through oxidation and combustion of NTA ligand during calcination at the high temperatures.

3.3.3. Co/CyDTA/SiO₂

FT-IR spectra of dried and calcined Co/CyDTA/SiO₂ are illustrated in Fig. 5C. Broad bands at 1652 cm^{-1} and 1630 cm^{-1} ($\delta\text{H}_2\text{O}$) were observed in the spectrum of the dried sample. The band at 1652 cm^{-1} was also observed in the spectrum of the catalysts calcined at 453–493 K, while the intensity of this band was gradually reduced with the calcination temperature. On the other hand, a new IR band emerged at 1590 cm^{-1} in the spectrum of Co/CyDTA/SiO₂ calcined at 453 K, and its intensity increased with the calcination temperature up to 493 K. Again, it is confirmed that these IR bands at 1652 and 1590 cm^{-1} are observed only when CyDTA coexists with Co nitrate by comparison with the spectrum of dried CyDTA/SiO₂ (Fig. 5C-h). These bands were ascribed to $\nu_{\text{as}}\text{COO}^-$ of the protonated CyDTA-Co complex and $\nu_{\text{as}}\text{COO}^-$ of the CyDTA-Co complex, respectively, as described below.

Assignment of IR bands for complexes of Co^{2+} with CyDTA in an aqueous solution is rather complicated because two types of CyDTA-Co complexes are formed depending on pH of the solution. It is reported that a $[\text{CoL}]^{2-}$ ($\text{L} = \text{CyDTA}$) complex is predominant in an aqueous solution under neutral and basic conditions, while a protonated one, namely $[\text{CoHL}]^-$, is stable in the aqueous solution under low pH (≤ 3) conditions [49]. According to this previous work, aqueous solutions containing CyDTA and Co nitrate with different pH of 2 and 11 (CyDTA- Co^{2+} molar ratio = 1) were prepared, and their FT-IR spectra were acquired for reference purposes. The reference spectrum of the solution with high pH (Fig. 5C-j) showed a weak band at 1590 cm^{-1} , which was attributed to $\nu_{\text{as}}\text{COO}^-$ of the $[\text{CoL}]^{2-}$ complex. Meanwhile, two bands observed at 1740 cm^{-1} and 1652 cm^{-1} in the reference spectrum of the solution with low pH (Fig. 5C-i) were assigned to νCO and $\nu_{\text{as}}\text{COO}^-$ of the $[\text{CoHL}]^-$ complex, respectively, in accordance with the literature [51]. The characteristic band at 1652 cm^{-1} was also observed in the spectrum of dried Co/CyDTA/SiO₂. Compared to the FT-IR spectra of the reference solutions, it is likely that interaction between CyDTA and Co^{2+} in the dried sample was similar to that of the $[\text{CoHL}]^-$ complex in an acidic environment. This interaction is preserved to some extent during calcination up to 493 K because the band at 1652 cm^{-1} was still observed in the spectrum of the catalyst calcined at 493 K. On the other hand, the emergence of the new IR band at 1590 cm^{-1} indicates the formation of different type of interaction between Co and CyDTA during calcination, which is similar to that of the $[\text{CoL}]^{2-}$ complex favorable in a neutral-basic environment.

Fig. 6 displays change in absorbance of the IR bands at 1590 and 1652 cm^{-1} as a function of the calcination temperature. The intensity of the band at 1590 cm^{-1} increased with increasing the calcination temperature in the range of 453–493 K where $I(\text{Co}2p_{3/2})/I(\text{Si}2p)$ for calcined Co/CyDTA/SiO₂ increased sharply.

3.4. Coordination environments of Co in dried and calcined catalysts

Coordination environments of Co in the dried and calcined catalysts, and the effect of the chelating agent on them were then studied by ex situ/in situ Co K-edge (Q)XAFS. Attentions were paid to clarify temperature-dependent structural perturbations of the complex formed in the chelate-assisted catalysts during calcination. Here, we present only (Q)XAFS results of Co/SiO₂ and Co/CyDTA/SiO₂ because there was only minor difference between those of Co/SiO₂ and Co/NTA/SiO₂.

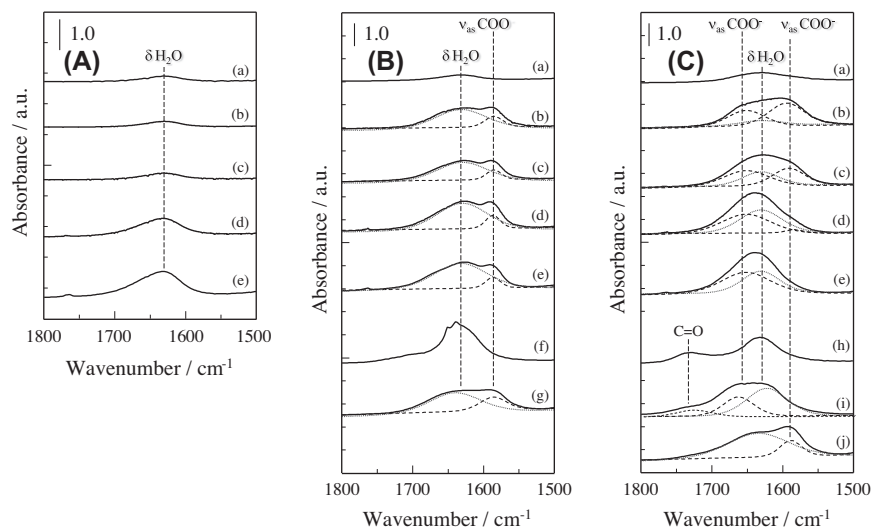


Fig. 5. Ex situ FT-IR spectra of Co/SiO₂ (A), Co/NTA/SiO₂ (B), and Co/CyDTA/SiO₂ (C) after drying and calcination at different temperatures. This figure also includes some reference spectra of dried L/SiO₂ (L = NTA, CyDTA) and aqueous solutions containing Co(NO₃)₂·6H₂O and L: After calcination at 523 K (a), 493 K (b), 473 K (c) and 453 K (d), after drying at 383 K (e), dried NTA/SiO₂ (f), Co(NO₃)₂·6H₂O + NTA soln. (pH = 10.2) (g), dried CyDTA/SiO₂ (h), Co(NO₃)₂·6H₂O + CyDTA soln. (pH = 1.5) (i), Co(NO₃)₂·6H₂O + CyDTA soln. (pH = 10.7) (j).

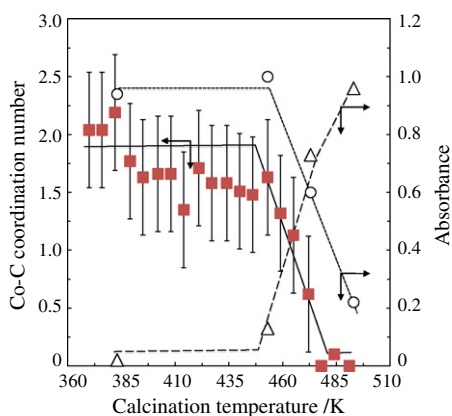


Fig. 6. Change in absorbance of the IR bands at 1590 cm⁻¹ (open triangle) and 1650 cm⁻¹ (open circle) observed in the ex situ FT-IR spectra of Co/CyDTA/SiO₂ after drying and calcination at different temperatures (see Fig. 5). This figure also illustrates change in the Co-C coordination numbers of the CyDTA-Co complex formed in the same catalyst (closed square). These numbers were determined by curve fitting analysis of in situ FT-EXAFS of Co/CyDTA/SiO₂ during TPO (for more detail see Section 3.4.2).

3.4.1. Co/SiO₂

3.4.1.1. Coordination environment of Co in dried catalyst. The coordination environment of dried Co/SiO₂ was studied by ex situ Co K-edge XAFS in our previous work [44]. It showed that both XANES and Fourier transformed $k^3\chi(k)$, hereafter simply denoted as FT-EXAFS, of this sample were similar to those of polycrystalline Co(NO₃)₂·6H₂O. Curve-fitting analysis confirmed that the coordination environment of Co species in dried Co/SiO₂ was similar to that of the hexaaqua Co (II) complex in which Co atom is surrounded by six H₂O molecules with a distorted octahedral structure [52].

3.4.1.2. Change in coordination environment of Co during calcination. Change in the coordination environment of Co during calcination was then studied by in situ Co K-edge QXAFS coupled with TPO. Fig. 7a illustrates change in Co K-edge FT-EXAFS of Co/SiO₂ during TPO. At low temperatures (366 ≤ T ≤ 426 K), only a broad peak attributed to the Co-O coordination shell of Co(NO₃)₂·nH₂O

($n \leq 6$) was observed at around 0.16 nm (not phase shift corrected). The intensity of this peak was reduced with increasing the calcination temperature, indicating that hydrating water is eliminated from Co nitrate species. It would also result from increasing thermal disorder caused by heating. On the other hand, three peaks appeared at 429 K. These three peaks are characteristic of Co₃O₄, and ascribed to the Co-O, Co-Co (Oh), and Co-Co (Td) coordination shells of Co₃O₄ [29,33]. In other words, the appearance of these three peaks is indicative of the formation of Co₃O₄ species. Fig. 8a displays change in partial pressures of CO₂ ($m/z = 44$) and NO₂ ($m/z = 46$) in tail gas from the in situ XAFS cell monitored by on-line MS. As displayed in this figure, NO₂ was observed in tail gas simultaneously with the appearance of the Co₃O₄ peaks in the FT-EXAFS spectra. These results clearly show that Co nitrate species were decomposed to form Co₃O₄ species at around 430 K.

At high temperatures (>430 K), the intensities of the Co-Co coordination peaks of Co₃O₄ species increased with increasing the temperature up to approximately 500 K, indicating that Co₃O₄ species are agglomerated in this temperature range.

3.4.2. Co/CyDTA/SiO₂

3.4.2.1. Coordination environment of Co in dried catalyst. Ex situ Co K-edge XANES of dried Co/CyDTA/SiO₂ is shown in Fig. 9. General features of this XANES spectrum were similar to those of polycrystalline Co(NO₃)₂·6H₂O. However, there also existed small difference between them; a weak shoulder peak was observed at around 7740 eV in the spectrum of dried Co/CyDTA/SiO₂, while such shoulder peak was absent from that of Co(NO₃)₂·6H₂O [44]. Since sub-stoichiometric amount of CyDTA was used for preparation of Co/CyDTA/SiO₂ (CyDTA-Co²⁺ molar ratio = 0.25), this difference could reflect coexistence of Co nitrate species and small amount of the CyDTA-Co complex. Pattern-fitting analysis was then performed using the XANES spectra of Co(NO₃)₂·6H₂O and dried Co-CyDTA/SiO₂, namely the co-impregnation catalyst. Note that all the Co in the co-impregnated catalyst is involved in the formation of the 1:1 complex with CyDTA [28,29]. EXAFS analysis also revealed that the coordination environment of Co in this co-impregnated catalyst was similar to that of the protonated complex. As illustrated in Fig. 9, the XANES spectrum of dried

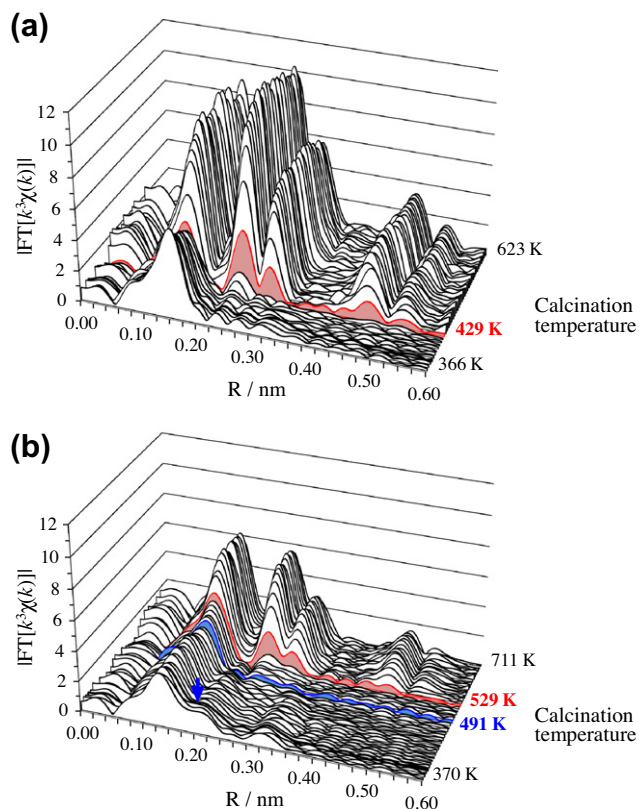


Fig. 7. Change in Co K-edge FT-EXAFS of Co/SiO₂ (a) and Co/CyDTA/SiO₂ (b) during calcination monitored by in situ QXAFS technique. The sample was heated from 373 to 623 K at a ramp rate of 1 K min⁻¹ followed by 10 K min⁻¹ in the range of 623–723 K under flowing 20% O₂/He (99.99995%, approximately 100 mL min⁻¹). XAFS spectra were acquired at every 180 s.

Co/CyDTA/SiO₂ was fitted well with those of Co(NO₃)₂·6H₂O and dried Co–CyDTA/SiO₂. Pattern-fitting analysis also showed that about 20% of the total Co in dried Co/CyDTA/SiO₂ was involved in the complex formation. This means that almost all CyDTA form the complex with Co²⁺ in dried Co/CyDTA/SiO₂ because a maximum amount of Co that can be involved in the 1:1 complex formation is one-fourth of the total Co in this sample.

3.4.2.2. Change in coordination environment of Co during calcination.

In the FT-EXAFS of Co/CyDTA/SiO₂ during TPO (Fig. 7b), two peaks were observed in low and middle temperature ranges (370 K ≤ T < 491 K). A main peak was attributed to ill-resolved

overlapping Co–O coordination shells of Co nitrate species and the protonated complex by comparison with FT-EXAFS spectra of Co(NO₃)₂·6H₂O and dried Co–CyDTA/SiO₂ (not shown here), while a shoulder peak at around 0.23 nm (phase shift not corrected) was originated from the Co–C coordination shell of the complex (indicated by an arrow in Fig. 7b). The intensity of the Co–C coordination peak was almost constant up to 440–450 K, while it turned to decline above this temperature. This coordination peak was not observed in the FT-EXAFS spectrum acquired at 491 K. It is noted that the intensity of the Co–O coordination peaks is fairly constant in this temperature range. Therefore, it is unlikely that disappearance of the Co–C coordination peak is due to increasing thermal disorder induced by heating. To get a more quantitative insight, the Co–C coordination numbers were calculated by curve fitting analysis and are plotted against the calcination temperature (see Fig. 6). In spite of large experimental errors, an overall trend is clearly seen from this figure; the Co–C coordination number started to decline at around 450 K and dropped almost zero at around 480 K. Since the IR bands originated from the complexes were still observed in the ex situ FT-IR spectra of Co/CyDTA/SiO₂ calcined at 453–493 K, decrease in the Co–C coordination number represents change in the coordination environment of the protonated complex formed in the dried Co/CyDTA/SiO₂ rather than combustion of CyDTA ligands.

To confirm this point more explicitly, change in partial pressures of CO₂ and NO₂ in tail gas during the QEXAFS experiment of Co/CyDTA/SiO₂ is shown in Fig. 8b. An intense peak of CO₂ formation was observed in the temperature range of 490–550 K, which was accompanied with NO₂ formation. Therefore, these peaks are attributed to the combustion of CyDTA ligand and/or its derivative. In other words, they are still present in the catalyst in the calcination temperature range of 450–480 K. Since the Co–C coordination number changed in a similar way to that observed for the IR band at 1652 cm⁻¹ and decreased with increasing absorbance of the IR band at 1590 cm⁻¹ as illustrated in Fig. 6, change in the coordination environment of the complex would be closely related with an occurrence of different type of interaction between Co and CyDTA as revealed by ex situ FT-IR. NO₂ formation was also observed at around 480 K, which should be attributed to decomposition of Co nitrate species. This decomposition temperature is higher than that observed for Co/SiO₂, but still lower than that reported for thermal decomposition of polycrystalline Co(NO₃)₂·6H₂O [53]. Since the $I(\text{Co}2p_{3/2})/I(\text{Si}2p)$ for dried Co/CyDTA/SiO₂ was smaller than that for dried Co/SiO₂ as illustrated in Fig. 4, it is suggested that agglomeration of Co nitrate species in dried Co/CyDTA/SiO₂ is responsible for the higher temperature required for their decomposition during TPO.

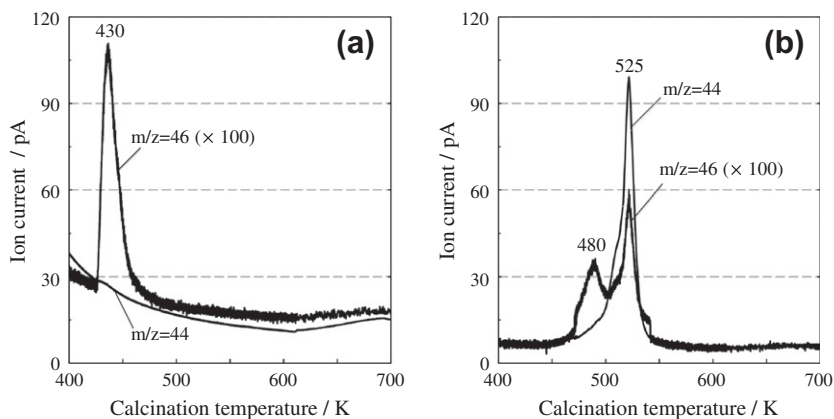


Fig. 8. Change in partial pressures of CO₂ ($m/z = 44$) and NO₂ ($m/z = 46$) in the tail gas from in situ XAFS cell monitored by the on-line MS spectroscopy; Co/SiO₂ (a) and Co/CyDTA/SiO₂ (b).

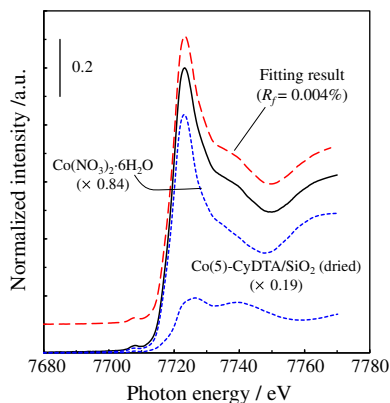


Fig. 9. Pattern-fitting result of the ex situ Co K-edge XANES of dried Co/CyDTA/SiO₂ (solid line) using those of polycrystalline Co(NO₃)₂·6H₂O and dried Co–CyDTA/SiO₂ (broken lines). The R^2 value defined by Eq. (3) is also indicated to show goodness of the fitting.

In the FT-EXAFS of Co/CyDTA/SiO₂ acquired at 529 K, three peaks characteristic of Co₃O₄ species were observed. It is highlighted that the formation of Co₃O₄ species took place simultaneously with the combustion of CyDTA ligand. This means that there is an obvious temperature gap between decomposition of Co nitrate species and formation of Co₃O₄ species in Co/CyDTA/SiO₂. Such temperature gap was never observed during the QEXAFS experiment of Co/SiO₂. Once Co₃O₄ species were formed, the intensities of the Co–Co coordination peaks of Co₃O₄ species increased with the calcination temperature. However, their intensities were no more than 50–60% of those observed in the QEXAFS spectra of Co/SiO₂ at the high temperatures. This indicates that agglomeration of Co₃O₄ species was retarded in Co/CyDTA/SiO₂, which is consistent with ex situ XRD and XPS results.

4. Discussion

Our previous works demonstrated that the two-step impregnation method using the chelating agents such as NTA and CyDTA improved the FTS activity of 20 mass% Co/SiO₂ effectively [30–33]. Use of CyDTA improved dispersion of Co⁰ as well, while it hardly affects high reducibility of Co for the catalyst prepared in the absence of the chelating agents (96%) [33]. It is also worth noting that only small amounts of CyDTA, namely the CyDTA–Co²⁺ molar ratio of 0.25–0.5, were necessary for enhancing the FTS activity of the catalyst prepared using CyDTA. This suggested that only a part of Co²⁺ in the dried catalyst was involved in the complex formation with CyDTA. In other words, surplus Co would remain as Co nitrate before calcination. Seemingly, this is reminiscent of the results of the catalysts prepared using the mixed salt of Co nitrate and Co acetate [11] rather than those of the catalysts prepared by the co-impregnation method using the chelating agents, while use of the mixed salt as the precursor lowered reducibility of Co. Ex situ XRD and Co K-edge EXAFS analyses of the calcined catalysts also revealed that CyDTA had ability to decrease size of Co₃O₄ species without forming detectable quantities of Co silicate-like species [33], and provided indirect evidence that some kind of interaction would be formed between Co nitrate and the complex during drying and/or calcination. However, formation mechanism of small precursor oxides during calcination of chelate-assisted Co/SiO₂ has not been fully understood yet.

In this work, 20 mass% Co/SiO₂ were prepared by this two-step impregnation method using several chelating agents, and the effects of the calcination temperature and chelating agent on their catalytic activities and coordination environments of Co species

were studied by activity test and in situ QXAFS in conjunction with several ex situ characterization techniques. It was revealed that the high calcination temperatures (>473 K) and large complex formation constants ($\log K_{\text{Co}} \geq 16$) of the chelating agent were crucial for effective enhancement of both the FTS activity and dispersion of Co₃O₄ species formed in the calcined catalyst. Finally, we discuss mechanistic aspects of the role of the chelating agents, NTA and CyDTA, based on the in situ and ex situ characterization results.

4.1. Role of CyDTA

4.1.1. Effect of CyDTA on surface structure of dried Co/CyDTA/SiO₂

The ex situ FT-IR spectrum of dried Co/CyDTA/SiO₂ indicated the presence of interaction between Co and CyDTA, which was similar to that of the protonated CyDTA–Co complex, namely [CoHL][−] (L = CyDTA), in the aqueous solution. Ex situ XANES analysis of the same sample also confirmed that about one-fourth of the total Co in dried Co/CyDTA/SiO₂ were involved in the complex formation with CyDTA, while remaining species were present as Co nitrate. This means that almost all CyDTA in the dried sample form the [CoHL][−] complex after drying due to its strong affinity with Co²⁺ because the CyDTA–Co molar ratio of this catalyst is 0.25. The formation of the protonated complex in the dried sample is also reasonable in view of the solution chemistry in the Co²⁺–CyDTA system [49] because the acidic Co nitrate solution with approximate pH 3 was impregnated before drying. Although exact coordination structures of the complexes in the aqueous solutions are still unknown yet, it is reasonable to assume that the [CoL]^{2−} complex has a six (or seven) coordination structure according to single crystal XRD studies on Ca[Fe(OH₂)L]₂·8H₂O [54] and [Na₆(NO₃)₂(H₂O)₁₃][NiL]₂ [55], while the protonated one has a five (or six) coordination structure with one free carboxyl group. Furthermore, our previous works on the co-impregnated Co–CyDTA/SiO₂ revealed that the complex formed in the impregnated and dried samples had stronger affinity with surface hydroxy group than Co nitrate [28] which indicates that the [CoHL][−] complex in dried Co/CyDTA/SiO₂ interacts with the surface hydroxy group as well. Since the PZC of SiO₂ surface is around 2 [56], Si–OH species would be a stable form in dried Co/CyDTA/SiO₂. Therefore, it is unlikely that the free carboxyl group of the protonated complex interacts with the surface hydroxy group. Instead, it is probable that unsaturated Co²⁺ of the [CoHL][−] complex is coordinated with Si–OH species as depicted in Scheme 1a. It is also stressed that, according to the literature reported by Zhuravlev [57], the surface O–H density of various amorphous SiO₂ samples with maximum degree of hydration is approximately 4.6–4.9 OH groups nm^{−2}, independent of the origin and structural characteristics of amorphous silicas. This surface density is comparable with that of the complex formed in dried Co/CyDTA/SiO₂ (approximately 2.4 complexes nm^{−2}). Thus, it is also reasonable that the [CoHL][−] complex formed in dried Co/CyDTA/SiO₂ spreads over support surface through the formation of the coordination bonds with the surface hydroxy groups. Conversely, strong affinity of the complex with surface hydroxy group means that only a part of Co nitrate can be involved in interaction with the surface hydroxy group, which would facilitate agglomeration of Co nitrate compared to the catalyst prepared without using the chelating agent. This is probably why the $I(\text{Co}2p_{3/2})/I(\text{Si}2p)$ for dried Co/CyDTA/SiO₂ was smaller than that for dried Co/SiO₂, and the former sample showed the lower FTS activity than the later one.

4.1.2. Interpretation of increase in $I(\text{Co}2p_{3/2})/I(\text{Si}2p)$ for calcined Co/CyDTA/SiO₂

During calcination of dried Co/CyDTA/SiO₂ at 453–523 K, sharp increase in the $I(\text{Co}2p_{3/2})/I(\text{Si}2p)$ was observed as illustrated in Fig. 4 which suggests that relatively large Co species in this sample

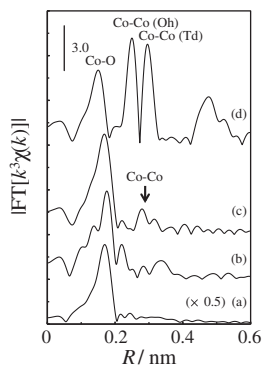


Fig. 10. Ex situ Co K-edge FT-EXAFS of Co/CyDTA/SiO₂ calcined at different temperatures in comparison with that of Co(NO₃)₂·6H₂O. XAFS spectra were measured at low temperatures (17–20 K) using a He cryostat; polycrystalline Co(NO₃)₂·6H₂O (a), dried Co/CyDTA/SiO₂ (b), Co/CyDTA/SiO₂ calcined at 473 K (c), Co/CyDTA/SiO₂ calcined at 523 K (d).

reduction of Co species observed in the similar calcination temperature range (453–523 K, see Fig. 4).

In this connection, it is worth citing studies by Che et al. [15,58] where they reported that dispersion of NiO species in calcined Ni/SiO₂ was enhanced by a two-step impregnation method using ethylenediamine (en). In their preparation method, the aqueous solution containing [Ni(en)₆]²⁺ complex was impregnated on SiO₂ first. This complex was converted into small Ni²⁺ species interacted with SiO₂ surface during 1st calcination. The aqueous solution of Ni nitrate was then impregnated on this sample followed by calcination. Their in situ Ni K-edge EXAFS results suggested that small Ni²⁺ species interacted with SiO₂ surface worked as anchoring sites for preventing agglomeration of Ni oxide species during 2nd calcination [58]. Different from en in their preparation method, the chelate complex itself plays a significant role in enhancing dispersion of Co in our two-step impregnation method.

4.1.4. Formation of Co silicate-like species during calcination and its importance

Once Co₃O₄ species were formed in Co/CyDTA/SiO₂, they started to agglomerate as indicated by decrease in the $I(\text{Co}2p_{3/2})/I(\text{Si}2p)$ in the calcination temperature range of 523–723 K. However, agglomeration of Co₃O₄ species in Co/CyDTA/SiO₂ was suppressed compared to that observed during calcination of Co/SiO₂. Since CyDTA ligand is already removed from the catalyst surface by combustion, a different mechanism should work for retarded agglomeration of Co₃O₄ species. In this regard, it is worth noting that the complex formed in co-impregnated Co–CyDTA/SiO₂ was selectively converted into Co silicate-like species after calcination at 723 K

[28,29]. It was considered that strong affinity of the complex with the surface hydroxy group as well as its high stability was responsible for selective formation of such silicate-like species. Girardon et al. [59] and Trujillano et al. [14,60] also reported that the formation of surface silicate is facilitated by use of organic Co precursor or the addition of organic ligands, respectively. To confirm the formation of Co silicate-like species in Co/CyDTA/SiO₂ during calcination, pattern-fitting analysis of in situ Co K-edge XANES spectra measured during TPO was carried out in two different ways; one was to fit them with two XANES spectra of polycrystalline Co₃O₄ and α -Co₂SiO₄, and the other was to use only one reference spectrum of polycrystalline Co₃O₄. Fig. 11 illustrates typical pattern-fitting results of the XANES spectrum of Co/CyDTA/SiO₂ acquired at 711 K. The quality of fitting was always improved by involving contribution of α -Co₂SiO₄ for the spectra of Co/CyDTA/SiO₂ measured in the range of 548–711 K. Pattern-fitting analysis also revealed that percentage of Co contributed to the silicate formation was 13–23%. In situ XANES spectra of Co/SiO₂ were, on the other hand, fitted with only one reference spectrum of polycrystalline Co₃O₄. Contribution from Co silicate was always negative when fitting analysis was carried out using two reference spectra of polycrystalline Co₃O₄ and α -Co₂SiO₄. These results suggested that the protonated complex in dried Co/CyDTA/SiO₂ was converted into Co silicate-like species after combustion of carbon network. These silicate species would work as anchoring sites for Co₃O₄ species formed from the Co_xO_y clusters, as suggested by Che et al. [15] and Lim et al. [61], resulting in controlled agglomeration of Co₃O₄ species during calcination at the high temperatures.

4.2. Role of NTA

As mentioned in 3.3.2, the ex situ FT-IR spectrum of dried Co/NTA/SiO₂ indicated the presence of interaction between Co and NTA which is similar to that of the [CoL][−] (L = NTA) complex in the aqueous solution. However, in situ/ex situ XAFS did not provide clear information about change in the coordination environment of the NTA–Co complex during calcination. It is reasonable to assume that only a small part of NTA is involved in the [CoL][−] complex formation due to its lower affinity with Co²⁺ compared to CyDTA, so the presence of the complex would not cause clear differences in the XANES and FT-EXAFS spectra. Presumably, the role of NTA is similar to that of CyDTA. Only a small part of Co (Co_xO_y) can be stabilized by the NTA complex during calcination, which works as the dispersion enhancer. On the other hand, remaining Co nitrate species are decomposed to form Co₃O₄ species followed by agglomeration at high calcination temperatures. These two different effects would offset each other, resulting in apparently constant $I(\text{Co}2p_{3/2})/I(\text{Si}2p)$ during calcination (Fig. 4).

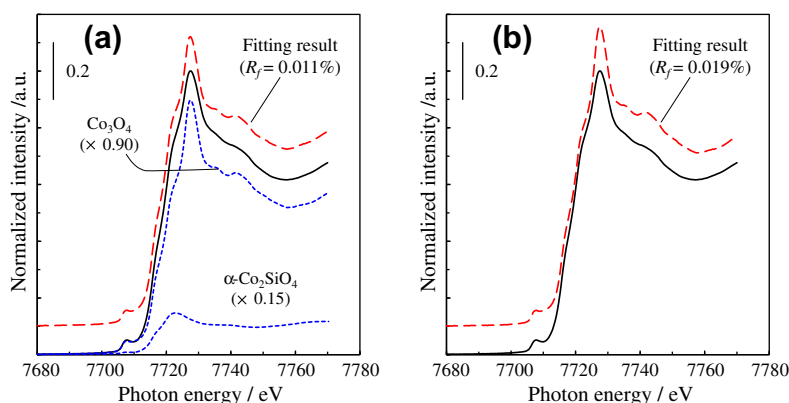


Fig. 11. Pattern-fitting results of the in situ Co K-edge XANES spectrum of Co/CyDTA/SiO₂ measured during TPO at 711 K. Fitting analysis was carried out using two reference spectra of polycrystalline Co₃O₄ and α -Co₂SiO₄ (a), and only one reference spectrum of polycrystalline Co₃O₄ (b).

5. Conclusion

In this work, 20 mass% Co/SiO₂ catalysts were prepared by the newly developed two-step impregnation method using several chelating agents. The effects of the calcination temperature and chelating agent on their FTS activities and surface structures were studied to deepen our understanding of the role of the chelating agents during preparation of the catalyst. The important results obtained in this work are summarized as follows.

- (1) The FTS activity of Co/L/SiO₂ prepared by a two-step impregnation method using the chelating agent (L) was dependent on the calcination temperature and increased with the calcination temperature in the range of 473–543 K when the chelating agents with strong affinity with Co²⁺ such as CyDTA were used for preparation.
- (2) Ex situ XRD and XPS revealed that size of Co species in calcined Co/CyDTA/SiO₂ was reduced with the calcination temperature in the range of 453–523 K, while those in calcined Co/SiO₂ were simply agglomerated to form Co₃O₄ species with low dispersion in the catalyst calcined at 723 K. CyDTA also had ability to suppress sintering of Co₃O₄ species during calcination at high temperatures.
- (3) Ex situ FT-IR and XAFS measurements also revealed that about one-fourth of the total Co in dried Co/CyDTA/SiO₂ were involved in the formation of the [CoHL]⁻ (L = CyDTA) complex, while remaining species were present as Co nitrate. Ex situ XAFS also indicated that there was no apparent interaction between them.
- (4) The results of in situ TPO-QEXAFS in conjunction with those of ex situ FT-IR and low-temperature EXAFS suggested that Co nitrate was decomposed during calcination of Co/CyDTA/SiO₂ at 460–500 K to form small Co_xO_y clusters which were stabilized by the Co–COO⁻ bond formation between the clusters and complexes. Such interaction was considered as the origin of size reduction of Co species during calcination at 453–523 K.
- (5) In situ TPO-QXAFS results of Co/CyDTA/SiO₂ also suggested that the complexes were converted to Co silicate-like species after combustion of carbon network. It was speculated that these silicate-like species worked as anchoring sites for preventing agglomeration of Co₃O₄ species formed from the Co_xO_y clusters during calcination at high temperatures.
- (6) The results obtained in this work demonstrated that specific interaction of the small Co oxide clusters from Co nitrate with chelate complexes is crucial for large activity enhancement induced by the chelating agent. Coexisting of both Co nitrate and the complex before calcination is essential for preparation of Co/SiO₂ catalyst by the two-step impregnation method using the chelating agents.

Acknowledgments

This research was supported by the Japan Society for the Promotion of Science (JSPS), Grant-in-Aid for Scientific Research (S), 17106011, 2005. EXAFS measurement was performed at the BL14B2 in the SPring-8 with the approval of JASRI (Proposal No. 2009B1835). We gratefully thank the staffs of SPring-8 for their technical support and their kind help.

References

- [1] E. Iglesia, Appl. Catal. A: Gen. 161 (1997) 59.
- [2] G.L. Bezemer, J.H. Bitter, H.P.C.E. Kuipers, H. Oosterbeek, J.E. Holeywijn, X. Xu, F. Kapteijn, A.J. van Dillen, K.P. de Jong, J. Am. Chem. Soc. 128 (2006) 3956.
- [3] J.P. den Breejen, P.B. Radstake, G.L. Bezemer, J.H. Bitter, V. Frøseth, A. Holmen, K.P. de Jong, J. Am. Chem. Soc. 131 (2009) 7197.
- [4] G. Prieto, A. Martínez, P. Concepción, R. Moreno-Tost, J. Catal. 266 (2009) 129.
- [5] J. van de Loosdrecht, S. Barradas, E.A. Caricato, N.G. Ngwenya, P.S. Nkwananya, M.A.S. Rawat, B.H. Sigwebela, P.J. van Berge, J.L. Visagie, Top. Catal. 26 (2003) 121.
- [6] Ø. Borg, E.A. Blekkan, S. Eri, D. Akporiaye, B. Vigerust, E. Rytter, A. Holmen, Top. Catal. 45 (2007) 39.
- [7] J.R.A. Sietsma, J.D. Meeldijk, P. den Breejen, M. Versluijs-Helder, A.J. van Dillen, P.E. de Jongh, K.P. de Jong, Angew. Chem. Int. Ed. 46 (2007) 4547.
- [8] W. Chu, L.-N. Wang, P.A. Chernavskii, A. Khodakov, Angew. Chem. Int. Ed. 47 (2008) 5052.
- [9] M. Wolters, L.J.W. van Grotel, T.M. Eggenhuisen, J.R.A. Sietsma, K.P. de Jong, P.E. de Jongh, Catal. Today 163 (2011) 12.
- [10] M. Kraum, M. Baerns, Appl. Catal. A: Gen. 186 (1999) 189.
- [11] S. Sun, N. Tsubaki, K. Fujimoto, Appl. Catal. A: Gen. 202 (2000) 121.
- [12] H. Ming, B.G. Baker, Appl. Catal. A: Gen. 123 (1995) 23.
- [13] E. van Steen, G.S. Sewell, R.A. Makhoshe, C. Mickelthwaite, H. Manstein, M. de Lange, C.T. O'Conner, J. Catal. 162 (1996) 220.
- [14] R. Trujillano, F. Villain, C. Louis, J.-F. Lambert, J. Phys. Chem. C 111 (2007) 7152.
- [15] M. Che, Z.X. Cheng, C. Louis, J. Am. Chem. Soc. 117 (1995) 2008.
- [16] L. Medici, R. Prins, J. Catal. 163 (1996) 38.
- [17] A.M. de Jong, V.H.J. de Beer, J.A.R. van Veen, J.W. Niemantsverdriet, J. Phys. Chem. 100 (1996) 17722.
- [18] T. Shimizu, K. Hiroshima, T. Honma, T. Mochizuki, M. Yamada, Catal. Today 45 (1998) 271.
- [19] Y. Ohta, T. Shimizu, T. Honma, M. Yamada, Stud. Surf. Sci. Catal. 127 (1999) 161.
- [20] R. Cattaneo, T. Weber, T. Shido, R. Prins, J. Catal. 191 (2000) 225.
- [21] G. Kishan, L. Coulier, V.H.J. de Beer, J.A.R. van Veen, J.W. Niemantsverdriet, Chem. Commun. (2000) 1103.
- [22] G. Kishan, L. Coulier, V.H.J. de Beer, J.A.R. van Veen, J.W. Niemantsverdriet, J. Catal. 196 (2000) 180.
- [23] L. Coulier, V.H.J. de Beer, J.A.R. van Veen, J.W. Niemantsverdriet, J. Catal. 197 (2001) 26.
- [24] R. Cattaneo, F. Rota, R. Prins, J. Catal. 199 (2001) 318.
- [25] F. Dumond, E. Marceau, M. Che, J. Phys. Chem. C 111 (2007) 4780.
- [26] T. Mochizuki, T. Hara, N. Koizumi, M. Yamada, Catal. Lett. 113 (2007) 165.
- [27] T. Mochizuki, T. Hara, N. Koizumi, M. Yamada, Appl. Catal. A: Gen. 317 (2007) 97.
- [28] T. Mochizuki, N. Koizumi, Y. Hamabe, T. Hara, M. Yamada, J. Jpn. Petrol. Inst. 50 (2007) 262.
- [29] N. Koizumi, T. Mochizuki, M. Yamada, e-J. Surf. Sci. Nanotechnol. 7 (2009) 633.
- [30] T. Mochizuki, D. Hongo, T. Satoh, N. Koizumi, M. Yamada, Catal. Lett. 121 (2008) 52.
- [31] T. Mochizuki, T. Sato, D. Hongo, N. Koizumi, M. Yamada, J. Jpn. Inst. Energy 87 (2008) 132.
- [32] N. Koizumi, T. Mochizuki, M. Yamada, Catal. Today 141 (2009) 34.
- [33] N. Koizumi, D. Hongo, Y. Ibi, Y. Hayasaka, M. Yamada, in: B.H. Davis, M.L. Occelli (Eds.), Advances in Fischer–Tropsch Synthesis, Catalysts and Catalysis, CRC Press, New York, 2009, pp. 95–118 (Chapter 6).
- [34] A.Y. Khodakov, J. Lynch, D. Bazin, B. Rebours, N. Zanier, B. Moisson, P. Chaumette, J. Catal. 168 (1997) 16.
- [35] J.-S. Girardon, E. Quinet, A. Griboval-Constant, P.A. Chernavskii, L. Gengembre, A.Y. Khodakov, J. Catal. 248 (2007) 143.
- [36] A.Y. Khodakov, A. Griboval-Constant, R. Bechara, F. Villain, J. Phys. Chem. B 105 (2001) 9805.
- [37] F. Morales, F.M.F. de Groot, P. Glatzel, E. Kleimenov, H. Bluhm, M. Ha1vecker, A. Knop-Gericke, B.M. Weckhuysen, J. Phys. Chem. B 108 (2004) 16201.
- [38] A.Y. Khodakov, Catal. Today 144 (2009) 251.
- [39] G. Jacobs, J.A. Chaney, P.M. Patterson, T.K. Das, B.H. Davis, Appl. Catal. A: Gen. 264 (2004) 203.
- [40] W. Chu, P.A. Chernavskii, L. Gengembre, G.A. Pankina, P. Fongarland, A.Y. Khodakov, J. Catal. 252 (2007) 215.
- [41] G. Jacobs, P.M. Patterson, Y. Zhang, T.K. Das, J. Li, B.H. Davis, Appl. Catal. A: Gen. 233 (2002) 215.
- [42] T.K. Das, G. Jacobs, P.M. Patterson, W.A. Conner, J. Li, B.H. Davis, Fuel 82 (2003) 805.
- [43] G. Jacobs, T.K. Das, P.M. Patterson, J. Li, L. Sanchez, B.H. Davis, Appl. Catal. A: Gen. 247 (2003) 335.
- [44] N. Koizumi, S. Suzuki, Y. Ibi, Y. Hayasaka, Y. Hamabe, T. Shindo, M. Yamada, J. Synch. Rad. 19 (2012) 74.
- [45] A.L. Ankudinov, B. Ravel, J.J. Rehr, S.D. Conradson, Phys. Rev. B 58 (1998) 7565.
- [46] A. Lapidus, A. Krylova, J. Rathousky, A. Zukal, M. Jancalkova, Appl. Catal. A: Gen. 80 (1992) 1.
- [47] A.R. Belambe, R. Oukaci, J.G. Goodwin Jr., J. Catal. 166 (1997) 8.
- [48] N. Tsubaki, K. Yoshii, K. Fujimoto, J. Catal. 207 (2002) 371.
- [49] T. Sato, Thesis, Tohoku University, 2007.
- [50] Y. Tomita, K. Ueno, Bull. Chem. Soc. Jpn. 36 (1963) 1069.
- [51] D.H. Busch, J.C. Bailar Jr., J. Am. Chem. Soc. 75 (1953) 4574.
- [52] F. Bigoli, A. Braibanti, A.P. Camellini, M.T. Camellini, Acta Crystallogr. B27 (1971) 1427.
- [53] C. Ehrhardt, M. Gjikaj, W. Brockner, Thermochem. Acta 432 (2005) 36.
- [54] G.H. Cohen, J.L. Hoard, J. Am. Chem. Soc. 88 (1966) 3228.
- [55] Y.X. Long, L.S. Long, R.B. Huang, L.S. Zheng, S.W. Ng, Acta Crystallogr. E61 (2005) m790.

- [56] G.A. Parks, Chem. Rev. 65 (1965) 177.
- [57] L.T. Zhuravlev, Langmuir 3 (1987) 316.
- [58] J.C. Yang, Y.G. Shul, C. Louis, M. Che, Catal. Today 44 (1998) 315.
- [59] J.-S. Girardon, A.S. Lermotov, L. Gengembre, P.A. Chernavskii, A.G. Constant, A.Y. Kohdakov, J. Catal. 230 (2005) 339.
- [60] R. Trujillano, J.-F. Lambert, C. Louis, J. Phys. Chem. C 112 (2008) 18551.
- [61] S. Lim, C. Wang, Y. Yang, D. Ciuparu, L. Pfefferle, G.L. Haller, Catal. Today 123 (2007) 122.